• reprinted from INELASTIC BEHAVIOR OF
• SOLIDS (M.F. KANNINEN ET AL. EDS.)
• McGRAW-HILL, 1970.

THE ROLE OF LARGE CRACK TIP GEOMETRY CHANGES IN PLANE STRAIN FRACTURE

James R. Rice and

M. Arthur Johnson*

Division of Engineering
Brown University
Providence, Rhode Island

ABSTRACT

Inclusion of large geometry change effects in crack tip stress analysis reveals features quite different from those anticipated through conventional treatments based on small geometry change (sgc) assumptions. Further, these features appear central to relating continuum stress analyses to microstructural failure mechanisms in the prediction of fracture toughness. Recent progress in the

*Presently at Eastman Kodak Company, Rochester, N.Y.

elastic-plastic sgc analysis of cracks in plane strain is first summerized. The paradoxical lack of intense straining directly ahead of a sharp crack tip, as required for ductile fracture mechanisms, disappears when actual large geometry changes in progressive crack tip blunting are included. An application of rigid plastic slip line theory is justified in the nonhardening case for treatment of the large but localized deformations, with the sgc solutions setting boundary conditions. Examples are worked out for small scale contained yielding and a fully plastic case. Fracture strength predictions based on a critical strain at a mean inclusion spacing distance from the tip agree rather favorably with available data, and a more elaborate ductile fracture model involving void growth and coalescence with the tip is studied. Enormous stress levels are predicted ahead of a crack tip in the sgc solutions, with tip stress singularities resulting for hardening materials. But these occur more through hydrostatic stress elevation than hardening in the conventional sense. Triaxiality cannot be maintained locally as the tip blunts. The net conclusion of the analysis is that maximum achievable stress levels are essentially limited, even with continuous strain hardening. This is suggestive of abrupt toughness transitions with temperature and loading rate when brittle stress controlled mechanisms (cleavage microcracking) lead to fracture, for the maximum achievable stress associated with a stress-strain relation for local conditions may be insufficient to the task.

1. INTRODUCTION AND SYNOPSIS

This paper addresses the problem of relating elastic-plastic stress analyses of cracked structures to microstructural fracture mechanisms, so as to predict criteria for crack extension in metals. Attention is limited to plane strain conditions. As suggested by the title, proper treatment of finite crack tip geometry changes is necessary to the task. In fact, we claim that effects which become apparent only in a full nonlinear treatment, geometric as well as constitutive, are central to the understanding of plane strain fracture.

Substantial progress has been made in recent years in analyzing stress and deformation fields near cracks in elastic-plastic materials. Solutions have been based on the conventional small geometry change assumptions, and will be summarized in the next section. Two important modifications of the results of these solutions become apparent when the actual large geometry changes at the tip are considered. First, no severe strain concentration results

directly ahead of a sharp crack tip, according to the small geometry change (sgc) solution for a nonhardening or moderately hardening material. Nevertheless, an opening displacement at the tip is predicted. When we include the actual large geometry changes in progressive blunting of the tip, quite a different picture emerges. Intense strains do now result directly ahead over a region comparable in size to the opening displacement. The relevance becomes clear upon examination of some fracture data. We see that the predicted extent of the large strain region at fracture is indeed comparable to typical microstructural size scales for fracture, such as mean inclusion spacing, grain size, etc.

The analysis of these large geometry changes is given in some detail later for a nonhardening material. It is argued that the rigid-plastic slip line theory may be used, with the sgc solution for a sharp tip crack employed to set boundary conditions. In addition, an approximate (and somewhat inadequate) prediction of ductile fracture strength is made by combining this analysis with some recent results on the ductile enlargement of cavities in macroscopically homogeneous deformation fields. Also, the possibility of geometric instabilities in the blunting analysis is discussed.

The second modification due to large crack tip geometry changes has to do with the stress distribution. The sgc solutions predict enormous stresses directly ahead of a crack in plane strain. Three times the simple tension yield value results for a nonhardening Mises material. Strain hardening results in even higher stresses and, as might be expected, the stress acting on the line directly ahead of the tip becomes infinite in the limit for a continuously hardening material. But, as implied by our noting the absence of large strains ahead, these large stresses do not occur by hardening in the conventional sense, but rather by alterations in the ratio of hydrostatic to uniaxial flow stress. Proper imposition of boundary conditions on the deformed crack tip prohibits such a large hydrostatic stress elevation there and in the immediate vicinity. The net conclusion is that the maximum stress achievable over any reasonable size scale is limited, even with continuous strain hardening. Some estimates of modified stress distributions are given. This effect is suggestive of an abrupt toughness transition with temperature or loading rate when stress-dominated mechanisms (e.g., cleavage microcracking) control fracture, for the stress-strain curve corresponding to local temperature and strain rate may lead to a maximum achievable stress insufficient to the task.

2. SUMMARY OF STRESS ANALYSIS FOR CRACKS UNDER PLANE STRAIN CONDITIONS

We consider bodies under loads symmetric to the crack line, so that only the tensile opening mode of relative crack surface displacement results. The important feature of all linear elastic analyses of such problems is that a characteristic inverse square root singularity results at the tip, so that the stresses in the homogeneous and isotropic case are[1]

$$\sigma_{\theta\theta} + \sigma_{rr} = \frac{1}{\nu}\sigma_{zz} = \frac{2K}{(2\pi r)^{1/2}}\cos\frac{\theta}{2} + \text{terms bounded at the tip}$$

$$\sigma_{\theta\theta} - \sigma_{rr} + 2i\sigma_{r\theta} = \frac{iK}{(2\pi r)^{1/2}}\sin\theta\,\exp\frac{i\theta}{2} + \text{terms bounded at the tip} \tag{1}$$

Here the components are referred to a cylindrical polar system, $\theta = \pm\pi$ being the crack faces, ν is the Poisson's ratio, and i is the imaginary unit number. K is Irwin's stress intensity factor. It equals $\sigma_\infty(\pi l/2)^{1/2}$ for the Inglis configuration of a crack of length l in an infinite body under remote tension σ_∞. Solutions are also known for many other cases.[2] The elastic singularity reflects general features which persist in the elastic-plastic case. The principal in-plane shear stress, which essentially governs yielding in plane strain, is half the magnitude of the latter stress combination. It is seen to vanish directly ahead of the crack while achieving its greatest values above and below the tip at $\theta = \pm\pi/2$.

Progress in understanding the elastic-plastic case began with asymptotic analyses of the near tip field, which have recently guided and been supplemented by accurate finite-element numerical solutions, whereas the fully plastic cases have been studied for many years on the basis of the slip line theory. Most of our attention will be directed to the nonhardening idealization. For contained yielding, Rice[3] noted the relevance of the Prandtl slip line field (Fig. 1) in providing the stress state near a sharp crack tip as $r \to 0$, in an isotropic perfectly plastic material (also, see Cherepanov[4]). As illustrated, constant stress regions A and B result over 45° wedges ahead and behind the tip. The centered fan C joining these regions has radial lines as principal shear directions, and results in a steady increase in mean normal stress from A to B so that the maximum tension directly ahead of the tip is

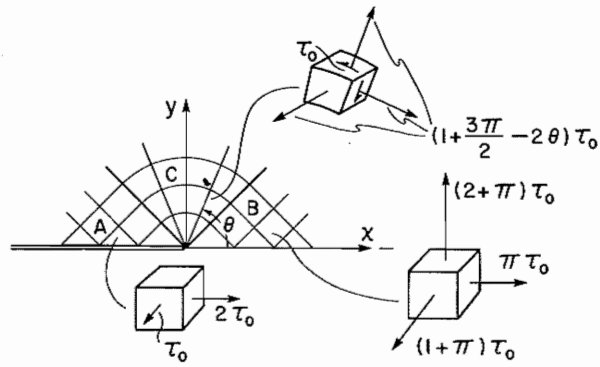

Fig. 1 *Slip line construction of stress state as $r \to 0$, for contained plane strain yielding of a nonhardening material.*[3]

$$\sigma_{yy}(\text{region B}) = (2 + \pi)\tau_o \approx 3\sigma_o \tag{2}$$

Here τ_o is the yield stress in pure shear and, as will be adopted elsewhere in this paper, the Mises form is employed in converting to the tensile yield stress σ_o.

Lack of focusing of slip lines in region B leads to no intense strain concentration as the tip is approached from directly ahead. However, one may show that the shear strain component $\gamma_{r\theta}$ (only) becomes infinite as $1/r$ when the tip is approached through the fan C

$$\gamma_{r\theta}(\text{region C}) \to \frac{\text{a function of } \theta}{r} = \gamma_o \frac{R(\theta)}{r} \tag{3}$$

The undetermined function of θ is written as $\gamma_o R(\theta)$, where γ_o $(= \tau_o/\text{shear modulus})$ is the initial yield strain. $R(\theta)$ measures the strength of the singularity at angle θ and may be interpreted as a distance over which the strain falls to a value comparable to γ_o. Hence, it is a very approximate measure of the distance to the elastic-plastic boundary. We will see that knowledge of this function from the sgc solution is essential for treating the large tip geometry change problem.

The sgc solution leads to a variation of displacements with θ at $r = 0$ in the centered fan, so that a discrete opening displacement is predicted at the tip. Cartesian components, measured from zero displacement as the tip is approached from directly ahead, at $r = 0$ are[3]

$$u_y(\theta) = \gamma_o \int_{\pi/4}^{\theta} R(\phi) \sin\phi d\phi \qquad u_x(\theta) = \gamma_o \int_{\pi/4}^{\theta} R(\phi) \cos\phi d\phi \tag{4}$$

and thus the crack tip opening displacement, defined as the total separation distance between the upper and lower crack surfaces, is

$$\delta_t = 2\gamma_o \int_{\pi/4}^{3\pi/4} R(\phi) \sin\phi d\phi \tag{5}$$

We will later wish to concentrate on the radial velocity component at $r = 0$ in the centered fan. The opening displacement will be taken as the measure of "time" so that $v_r = \partial u_r/\partial\delta_t$ and similarly for all other (dimensionless) velocities. $R(\theta)$ will, of course, depend on the applied load and we may convert this to dependence on the opening displacement, once δ_t is known in terms of load, writing $R(\theta) = R(\delta_t, \theta)$. In this notation the radial velocity at $r = 0$ according to sgc solutions is

$$v_r = v_r(\delta_t, \theta) = \gamma_o \int_{\pi/4}^{\theta} \frac{\partial R(\delta_t, \phi)}{\partial \delta_t} \cos(\theta - \phi)\, d\phi \tag{6}$$

According to the slip line velocity equations, the radial lines of the centered fan transmit a radial velocity independent of r, so that this equation also applies away from the crack tip.

The difficulty is that no exact solutions for $R(\delta_t, \theta)$ are available for contained yielding. We shall use a number of approximations for small scale yielding. This is a boundary layer formulation of the elastic-plastic problem in which the characteristic elastic singularity (Eq. (1)) is employed to set asymptotic boundary conditions at large distances from the tip[3,5] and provides a good approximation to complete solutions up to substantial fractions, say ½ to ¾, of net section yield load levels. There is only one characteristic length K^2/σ_o^2, so that $R(\delta_t, \theta)$ and δ_t are both proportional to this factor and the radial velocity (Eq. (6)) is therefore independent of δ_t. At the other extreme, we will also employ a fully plastic solution involving the Prandtl field and here again the velocity is independent of δ_t. Unfortunately, no results are available for the missing large-scale contained yielding range, in which case the velocity distribution will certainly vary with the opening displacement.

Guided by some etching studies, Rice[3] assumed a sinusoidal form for the amplitude of the singularity

$$R \approx R_{\max} \cos 2\left(\theta - \frac{\pi}{2}\right) \tag{7}$$

which is largest directly above the crack and falls to zero at the fan boundaries, and employed his path independent energy integral to solve for $R_{\max}$. The resulting approximation for small scale yielding is

$$\begin{aligned} R_{\max} &= \frac{3(1-\nu)}{4\sqrt{2}(2+\pi)}\left(\frac{K}{\tau_o}\right)^2 = 0.217\left(\frac{K}{\sigma_o}\right)^2 \\ \delta_t &= \frac{2(1-\nu^2)}{2+\pi}\frac{K^2}{E\tau_o} = 0.613\frac{K^2}{E\sigma_o} = 2.8\frac{\sigma_o}{E}R_{\max} \end{aligned} \tag{8}$$

Here, as subsequently, in giving numerical factors we take $\nu = 0.3$ and use the Mises shear-tension relation. The resulting radial velocity is

$$v_r = \frac{1}{2\sqrt{2}}\left[\cos\left(\theta - \frac{\pi}{4}\right) - \cos 2\left(\theta - \frac{\pi}{4}\right)\right] \tag{9}$$

Another approximation is provided by the nonhardening limit of the Hutchinson-Rice-Rosengren dominant singularity solution for a power-law hardening materal.[6,7] It is possible to solve for this limit analytically, although this was not noted in their papers. We omit all the lengthy details, simply noting that $R(\theta)$ is not symmetric about the y axis as assumed above, but rather attains its maximum at $\theta = 103.5°$ while still falling to zero at the fan boundaries, and that

$$\begin{aligned} R_{\max} &= 0.286\left(\frac{K}{\sigma_o}\right)^2 \\ \delta_t &= 0.717\frac{K^2}{E\sigma_o} = 2.5\frac{\sigma_o}{E}R_{\max} \end{aligned} \tag{10}$$

The velocity is

$$v_r = A\left\{\left(1 + \frac{3\pi}{2} - 2\theta\right)\left[\exp\left\{\left(\theta - \frac{\pi}{4}\right)\left(1 + \frac{5\pi}{4} - \theta\right)\right\} - \sqrt{2}\pi\mu(\theta)\right]\right.$$

$$\left. - \sqrt{2}(\cos\theta + \pi\sin\theta)\right\} \quad (11)$$

where $$\mu(\theta) = \int_{\pi/4}^{\theta} \sin\phi \exp\left[(\theta - \phi)\left(1 + \frac{3\pi}{2} - \theta - \phi\right)\right] d\phi$$

and $$A^{-1} = 2\sqrt{2}\exp\left[\left(1 + \frac{\pi}{2}\right)\frac{\pi}{2}\right] + 4\pi\mu\left(\frac{3\pi}{4}\right) - \sqrt{2}\pi$$

Conventional numerical methods of stress analysis (finite elements, finite differences) have been unsuccessful in providing the accuracy required near the crack tip singularity. In fact, most formulations have assigned a single nodal point to the crack tip so that the displacement variations known to occur there in the nonhardening case are prohibited. This difficulty was overcome in a finite element formulation of the small-scale yielding problem by Ostergren,[8] as guided by the features of the near tip field discussed above, and his procedure has recently been applied with a more refined mesh by Levy.[9] A system of four-sided finite elements is employed, with each bounded by coordinate lines of the type r = constant and θ = constant in a polar system, and having four nodal points at which displacements are prescribed. Those elements at the crack tip have two of their nodal points at the same physical point, so that different displacements result as the tip is approached along different radial lines. Further, a $1/r$ strain singularity results in the nearest tip elements whenever the nodal point displacements there are discontinuous. The procedure is quite suitable, based upon their results in the elastic case and from the close agreement with the Prandtl field stresses in the nearest tip elements in the perfectly plastic case. The results of their theses will be summarized in a forthcoming publication.

The values from Levy's work of R_{max} (which occurs at θ = 82.5–90°) and δ_t are

$$R_{max} = 0.155 \left(\frac{K}{\sigma_o}\right)^2$$

$$\delta_t = 0.425 \frac{K^2}{E\sigma_o} = 2.7 \frac{\sigma_o}{E} R_{max} \tag{12}$$

The radial velocity distribution is shown in Fig. 2 where it is compared with the previous two results and with a fully plastic case to be discussed shortly. The computer solution confirms the expectation that R_{max} should be comparable to the extent of the plastic zone. This solution, based on the Mises yield condition and $\nu = 0.3$, reveals an elastic-plastic boundary extending a maximum distance $0.175\ (K/\sigma_o)^2$ from the tip at $\theta = 70°$ and a distance $0.032\ (K/\sigma_o)^2$ directly ahead of the tip. The latter figure is expected to depend strongly on Poisson's ratio, perhaps vanishing when $\nu = 1/2$.

In contrast to the elastic case, no unique form for the crack tip singularity results in the fully plastic (limit load) case.[10] The deep

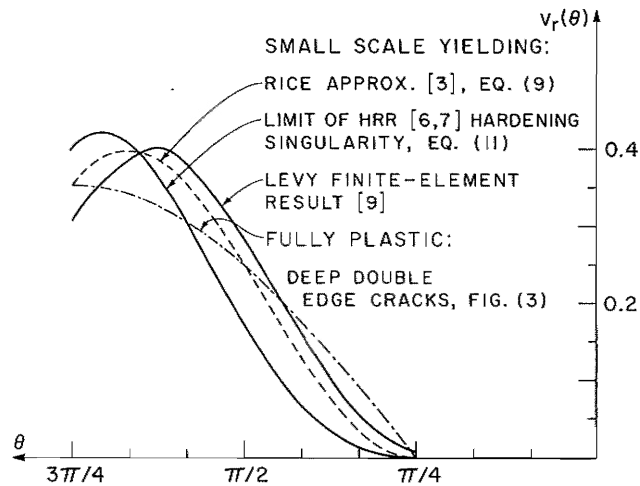

Fig. 2 *Velocity distribution (i.e., radial displacement rate with respect to crack opening displacement) in centered fan at crack tip, for various small scale yielding approximations and fully plastic case.*

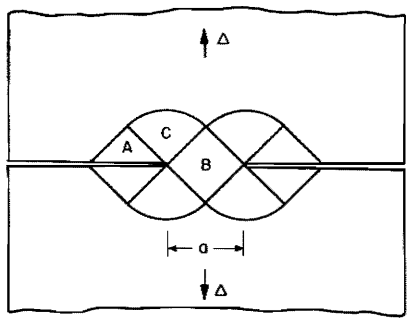

Fig. 3 *Slip line field at limit conditions for deep double edge cracks in plane strain.*

double edge notches of Fig. 3 maintain the Prandtl field and accompanying hydrostatic stress elevation at limit load, whereas the single edge notch or internal notch configurations do not. We shall examine the double edge notch case only, its similarity in stress state providing a basis for comparison with small scale yielding. The Prandtl field of Fig. 3 is the limiting sgc solution for an elastic-plastic material. However, in reporting results below, we neglect strains and displacements prior to limit conditions, which is the same as considering the material rigid-plastic. Although the initial yield strain γ_o then has no particular relevance, we continue to write the singularity in the form of Eq. (3) for comparison with the elastic-plastic results. Then it turns out that $R(\theta)$ = constant = $R_{\max}$ in the fan, where

$$R_{\max} = \frac{\sqrt{2}\Delta}{\gamma_o} \qquad \text{and} \qquad \delta_t = 4\Delta = 4.2\,\frac{\sigma_o}{E} R_{\max} \tag{13}$$

Here Δ is the displacement of the rigid portion of the specimen as in the figure. The radial velocity in the fan is

$$v_r = \frac{1}{2\sqrt{2}} \sin\left(\theta - \frac{\pi}{4}\right) \tag{14}$$

Incidently, these results are unique, in spite of the well-known lack of uniqueness for the entire velocity field in the deforming region.

Now, returning to the small scale yielding case, let us consider the stress acting directly ahead of the crack. Figure 4*a* was prepared from the computer solution for a nonhardening material. It is seen that σ_{yy} does attain the $3\sigma_o$ value at the tip predicted above, but the fall off in stress is very rapid, with approximately $2\sigma_o$ resulting

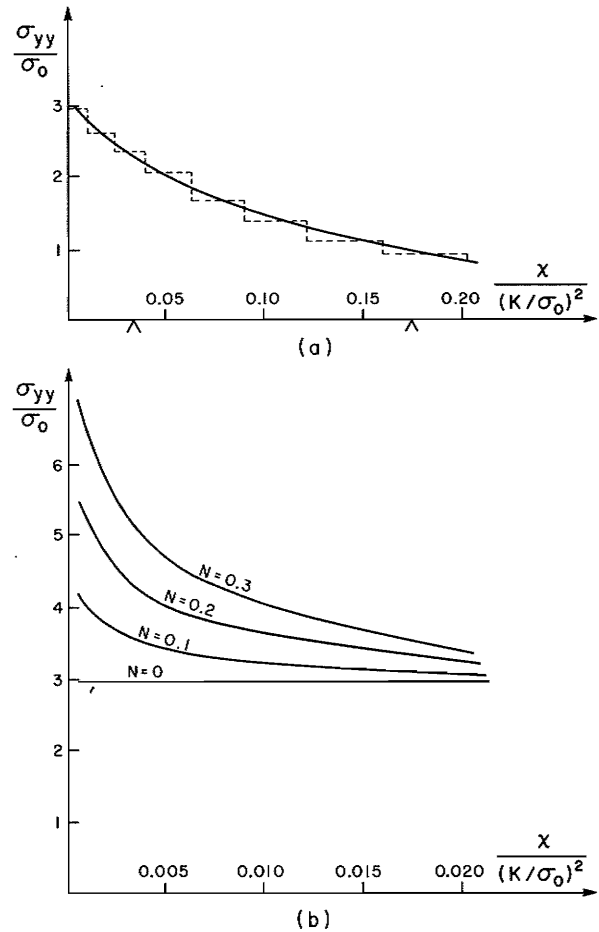

Fig. 4 *Stress acting directly ahead of crack under small scale yielding conditions: (a) from finite-element computer solution for a nonhardening material,*[8] *and (b) from singularity solution for materials hardening according to*[6,7] $\tau = \tau_o(\gamma/\gamma_o)^N$ *(note factor of 10 change in scale.*

at the point where the elastic-plastic boundary resides in front of the crack (first tick on x axis) and approximately σ_o resulting at a distance ahead equal to the maximum extent of the plastic zone (second tick).

Strain hardening may be brought into the description through the work of Hutchinson[6] and Rice and Rosengren.[7] They considered materials exhibiting a power-law relation

$$\tau = \tau_o \left(\frac{\gamma}{\gamma_o}\right)^N \tag{15}$$

between stress and strain in the hardening range $\gamma > \gamma_o$ and noted that the sgc solution for a sharp crack led to tip singularities of the form

$$\sigma_{ij} \to r^{-N/1+N} \Sigma_{ij}(\theta) \qquad \epsilon_{ij} \to r^{-1/1+N} E_{ij}(\theta) \tag{16}$$

In analogy to Eq. (3), the principal in-plane shear strain may be written in the form

$$\gamma \to \gamma_o \left[\frac{R(\theta)}{r}\right]^{1/1+N} \tag{17}$$

The form of $R(\theta)$ in the nonhardening limit $N \to 0$ has already been discussed in connection with Eqs. (10) and (11). In that case $\Sigma_{ij}(\theta)$ describes the Prandtl field. Similarly, for the practical range of hardening, $0 < N < 0.3$, the singularity amplitude is greatest above and below the tip but negligible ahead; $R(0)$ being typically of the order $10^{-2} R_{max}$ and zero when $N = 0$. The stress acting directly ahead of the crack, according to the dominant singularity solution, is shown in Fig. 4*b* for small-scale yielding conditions with various hardening exponents. Note that the scale on the x axis has been changed, so that we are now looking at a region having one-tenth the linear dimension of that examined in Fig. 4*a*. The complete computer solution shows a fall-off in stress not reflected in the dominant singularity solution; hence the horizontal line at $3\sigma_o$, representing the nonhardening case of $N = 0$, should be given a slight negative slope for agreement with Fig. 4*a*. Presumably, the as yet unavailable complete solutions with strain hardening would reveal a similar fall-off, so the other curves in Fig. 4*b* should be corrected in the same way.

3. PROGRESSIVE CRACK TIP BLUNTING

We have seen that the sgc solutions predict no intense strain concentration directly ahead of the tip. How does fracture occur there, particularly when ductile mechanisms operate and high stress alone is insufficient? We suggest that the prediction of an opening displacement, with consequent effects in modifying the strain distribution, is the key to the answer. Figure 5*a* shows a blunted crack tip and the

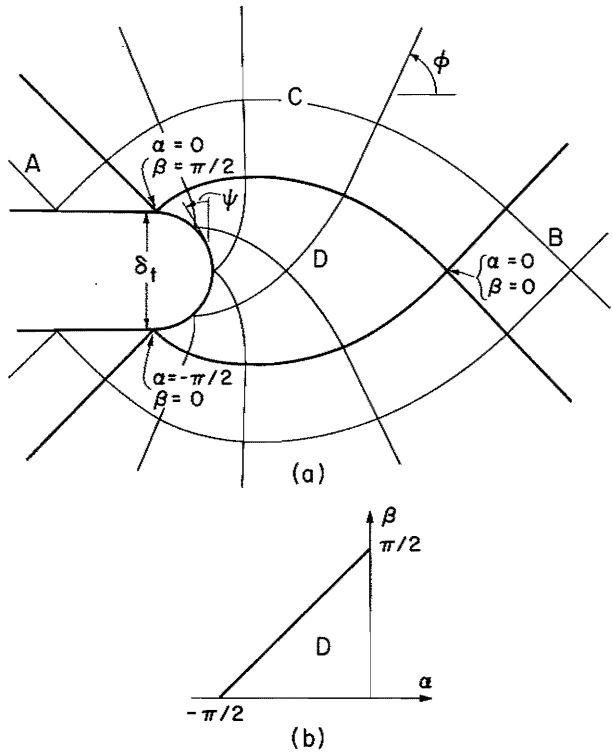

Fig. 5 *(a) Modification of slip line field in near tip region due to progressive blunting of crack tip with deformation (compare Figs. 1 and 3). (b) Map of region D into characteristic plane.*[12]

resulting change in the slip line field of Figs. 1 or 3. The constant stress regions A and B remain, and they continue to be joined by a fan C of straight slip lines. However, the fan is now noncentered and focuses intense strains into a region D directly ahead of the blunted tip. To appreciate the size scale involved, if the tip blunted into a semicircle of diameter δ_t, region D would have exponential spiral slip lines and would extend a distance $(e^{\pi/2} - 1)\,\delta_t/2 \approx 1.9\delta_t$ ahead of the tip.

As already hinted by the discussion of slip lines, we propose to treat the material as rigid-plastic for analysis of the large tip geometry changes. Also, an important approximation is suggested by the fact that the pertinent size scale is δ_t. This is of the order σ_o/E times the maximum extent of the plastic zone, and thus typically two orders of magnitude smaller. Since the straight slip lines of the fan transmit a uniform velocity parallel to themselves, velocities on the boundary

of region D are known in terms of velocities in the fan far away from the near tip perturbation. But when viewed on the larger size scale of plastic zone size, the tip still appears as a point, and hence velocities in the centered fan of the sgc solution should provide a good approximation to those in the noncentered fan of the finite geometry change solution. Thus the radial velocity $v_r(\theta, \delta_t)$ of the sgc solution provides boundary conditions for the blunting analysis, in that this may be taken as the normal velocity on the boundary of region D at the point of intersection by a straight slip line of the noncentered fan having an inclination angle equal to θ.

Following Hill's[11] treatment of slip line theory, and Wang's[12] earlier study of notch root deformation in a rigid-plastic case, we introduce a set of characteristic α, β coordinates in region D so that lines of β = const and α = const are, respectively, first and second principal shear directions. These are defined so that $\alpha = 0$ and $\beta = \phi - \pi/4$ (where ϕ is the first principal shear angle, Fig. 5*a*) on the upper boundary of region D, and that $\beta = 0$ and $\alpha = \phi - \pi/4$ on the lower boundary. As illustrated in Fig. 5*b*, region D maps into a fixed triangular region in the α, β plane. Letting $\sigma = (\sigma_{xx} + \sigma_{yy})/2$, equilibrium conditions of constancy of $\sigma - 2\tau_o \phi$ on α lines and of $\sigma + 2\tau_o \phi$ on β lines, together with boundary conditions, require that

$$\sigma = [1 + \pi + 2(\alpha - \beta)]\tau_o \qquad \phi = \alpha + \beta + \pi/4 \tag{18}$$

Letting v_α, v_β be velocity components in the α, β directions, the zero rate of extension condition for principal shear directions leads to

$$\frac{\partial v_\alpha}{\partial \alpha} - v_\beta = 0 \qquad \frac{\partial v_\beta}{\partial \beta} + v_\alpha = 0 \tag{19}$$

Boundary conditions on the velocity problem are given, within the approximation discussed above, by

$$\begin{aligned} v_\alpha(0, \beta) &= v_r(\theta) \text{ from sgc solution, with } \theta = \beta + \frac{\pi}{4} \\ v_\beta(\alpha, 0) &= -v_r(\theta) \text{ from sgc solution, with } \theta = -\alpha + \frac{\pi}{4} \end{aligned} \tag{20}$$

These equations determine the velocity field throughout region D as functions of α, β although we have yet to determine the physical coordinates of material points corresponding to a given α, β set. A

Riemann function method of solution may be employed for the velocity problem,[11,12] but direct finite difference integration of Eq. (19) along the characteristics is simpler and has been adopted in this study. One may write the velocity vector on the notch tip as a function of its tangent angle ψ (Fig. 5*a*) from this solution, since α and β as well as the direction of α and β lines on the tip are expressible in terms of ψ.

We will show shortly how the shape of the deformed notch tip may be determined directly from this velocity vector. Once the physical coordinates of points on the notch tip are known, we determine physical coordinates throughout region D as functions of α, β by solving the equations

$$\frac{\partial y/\partial \alpha}{\partial x/\partial \alpha} = -\frac{\partial x/\partial \beta}{\partial y/\partial \beta} = \tan\left(\alpha + \beta + \frac{\pi}{4}\right) \tag{21}$$

subject to the known values of x, y on the map of the notch tip into the α, β plane. Again, finite difference integration along characteristics is employed.

To locate the position of the deformed notch tip, let us write $\underline{n}(\psi)$ and $\underline{s}(\psi)$ as unit vectors at points on the tip, with the first in the normal direction and positive when pointing into the material, and with the second in the tangential direction and positive in the sense of increasing ψ. Then the velocity vector on the tip may be written in corresponding components as

$$\underline{v}(\psi,\delta_t) = v_n(\psi,\delta_t)\,\underline{n}(\psi) + v_s(\psi,\delta_t)\,\underline{s}(\psi) \tag{22}$$

Now we write the unknown position vector of points on the tip as functions of ψ and δ_t: $\underline{r} = \underline{r}(\psi,\delta_t)$. From the defintion of velocity

$$\frac{\partial \underline{r}}{\partial \delta_t} + \frac{\partial \underline{r}}{\partial \psi}\frac{\partial \psi}{\partial \delta_t} = \underline{v} \tag{23}$$

where $\partial\psi/\partial\delta_t$ is a derivative following a fixed material point. But $\partial\underline{r}/\partial\psi$ has a direction tangent to the notch tip, and, after dotting with $\underline{n}$ we have

$$\underline{n}(\psi)\cdot\frac{\partial \underline{r}(\psi,\delta_t)}{\partial \delta_t} = \frac{\partial}{\partial \delta_t}[\underline{n}(\psi)\cdot\underline{r}(\psi,\delta_t)] = v_n(\psi,\delta_t) \tag{24}$$

If we differentiate this equation with respect to ψ, noting that

$\partial \underline{n}/\partial\psi = \underline{s}$ and again that $\partial \underline{r}/\partial\psi$ is tangential to the notch tip, we have

$$\frac{\partial}{\partial \delta_t}[\underline{s}(\psi) \cdot \underline{r}(\psi, \delta_t)] = \frac{\partial v_n(\psi, \delta_t)}{\partial \psi} \tag{25}$$

Strictly speaking, the treatment thus far applies only to an initially sharp crack. However, the same analysis applies also as an approximation to the case of an initially blunt notch with tip position vector $\underline{r}(\psi, 0)$ before deformation, provided we are interested in states for which the plastic zone is large compared to the notch root size. The solution upon integration of the last two equations is

$$\underline{r}(\psi, \delta_t) = \underline{r}(\psi, 0) + \int_0^{\delta_t} \left[\underline{n}(\psi) + \underline{s}(\psi) \frac{\partial}{\partial \psi}\right] v_n(\psi, \delta_t)\, d\delta_t \tag{26}$$

For the specific cases which we consider here, the velocity vector does not depend on δ_t and therefore

$$\underline{r}(\psi, \delta_t) = \underline{r}(\psi, 0) + \left[\underline{n}(\psi) v_n(\psi) + \underline{s}(\psi) \frac{dv_n(\psi)}{d\psi}\right] \delta_t \tag{27}$$

Numerical results, summarized in graphical form in Fig. 6, are based on calculations with input velocity fields from the sgc analyses summarized in the last section. The shape of the blunted tip is shown as computed from Eq. (27) with the initial root

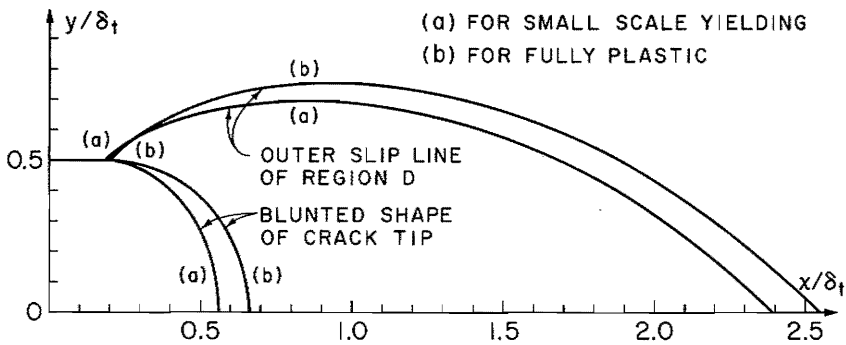

Fig. 6 *Predicted deformed shape of crack tip and outer slip line of region D for (a) small scale yielding as approximated in Eqs. (8) and (9), and (b) fully plastic.*

position vector $\underline{r}(\psi, 0) = 0$ (that is, for an initially sharp crack), as is also the shape of the shear lines forming the boundaries of region D. Figure 6*a* is for the input velocity field of Rice's[3] approximation for small scale yielding (summarized in Eqs. (8) and (9)). We shall henceforth take this field as representative of small scale yielding, although we must caution that an exact solution is not known and the two other analyses discussed in the last section lead to somewhat different results. Figure 6*b* is for the input velocity field from the fully plastic limit solution for deep double edge notches, Eqs. (13) and (14).

Let us now concentrate on the deformation along the x axis directly ahead of the crack tip. Referring to Fig. 5, we represent all quantities such as position, velocity, etc., parametrically in terms of the tangent angle ψ of the point on the notch tip intersected by the β slip line drawn from the point of interest on the x axis. Hence $\psi = \pi/2$ describes the point on the x axis at the outer extremity of region D and $\psi = 0$ describes the point at the deformed notch tip. From the velocity solution we know (numerically) the x direction velocity component along the x axis in the form

$$v_x(x, y)\Big|_{y=0} = V(\psi) \tag{28}$$

where $V(\psi)$ is dimensionless and vanishes at $\psi = \pi/2$. Similarly the x coordinate of a point corresponding to angle ψ may be written as (assuming an initially sharp crack)

$$x = \delta_t F(\psi) \tag{29}$$

where $F(\psi)$ is also dimensionless. Let X denote the position of a material point before deformation. Then $x = x(X, \delta_t)$ represents the deformed position, and we have

$$\frac{\partial x(X, \delta_t)}{\partial \delta_t} = F(\psi) + \delta_t F'(\psi) \frac{\partial \psi(X, \delta_t)}{\partial \delta_t} = V(\psi) \tag{30}$$

This equation may be integrated by setting $\psi(X, \delta_t) = \pi/2$ when $\delta_t = X/F(\pi/2)$, which is the opening displacement when a point initially a distance X from the tip first enters region D (we neglect the small distortions occurring ahead of region D, setting $x = X$ there). The result may be expressed in the form

$$X = \delta_t H(\psi) \quad \text{where} \quad H(\psi) = F\left(\frac{\pi}{2}\right) \exp\left\{-\int_{\psi}^{\pi/2} \frac{F'(\psi)\, d\psi}{F(\psi) - V(\psi)}\right\} \tag{31}$$

The deformation gradient is

$$\frac{\partial x(X, \delta_t)}{\partial X} = \delta_t F'(\psi) \frac{\partial \psi(X, \delta_t)}{\partial X} = \frac{F'(\psi)}{H'(\psi)} \tag{32}$$

If we let $\epsilon_x^{tr}, \epsilon_y^{tr}$ be "true" strains in the x and y directions on the line ahead of the tip, then ϵ_x^{tr} is log $\partial x/\partial X$ and $\epsilon_y^{tr} = -\epsilon_x^{tr}$ by incompressibility. Thus

$$\epsilon_y^{tr} = \log \frac{H'(\psi)}{F'(\psi)} = -\int_{\psi}^{\pi/2} \frac{V'(\psi)\, d\psi}{F(\psi) - V(\psi)} \tag{33}$$

By cross-plotting from numerical results, this can be expressed as a function of the initial coordinate of a material point through Eq. (31). The resulting true strain distributions as a function of X/δ_t are shown in Fig. 7 for the small scale yielding and fully plastic cases.

We see that large strains are indeed predicted directly ahead of a crack tip when the actual finite geometry changes are considered, but

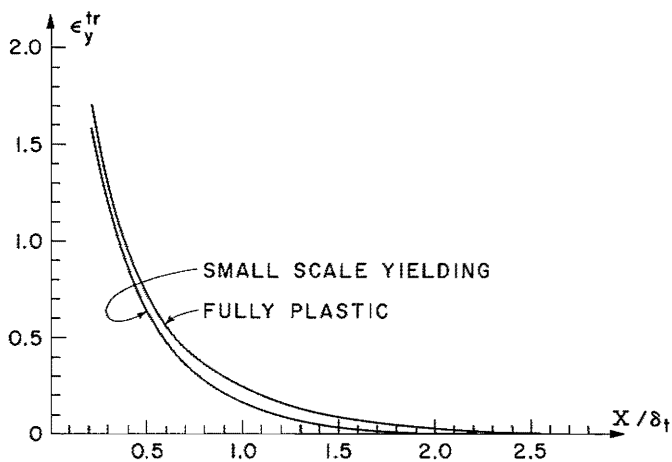

Fig. 7 *True strain on line ahead of crack, as a function of distance X of a material point from tip before deformation.*

only in the region adjacent to the blunting tip. This means that in situations for which large strains are required for fracture, as with ductile micromechanisms of void growth from inclusions,[13-16] the opening displacement at fracture must be such that the large strain region D envelops characteristic microstructural dimensions in the separation process. We shall analyze a rather detailed model for void growth and coalescence in the next section. For the moment, we adopt the simpler idea that some critical fracture strain must be achieved at a material point initially at distance X_o from the crack tip, where X_o might be identified as grain size or, better, a mean spacing of the larger second-phase inclusions responsible for ductile fracture.

It would seem plausible to assume that most structural metals would fracture at a true strain on this size scale between 0.2 and 1.0. Reading the corresponding values of X/δ_t from Fig. 7 and inverting the numbers, we therefore conclude that the crack opening displacement at fracture will be in the range

$$\delta_t \approx 1.0 \text{ to } 2.7\, X_o \tag{34}$$

If we adopt a wider range of true strain at fracture, say 0.1 to 2.0, to include cases of both unusually small and large ductility, the range spreads to $\delta_t \approx 0.8$ to $7.2\, X_o$. Since δ_t varies as K^2 in the small scale yielding case, the range of K is smaller. Drucker and Rice[17] have discussed trends which might be expected in different metals as based on the blunting affected region setting a size scale for large strains, with special reference to specimen size requirements for low nominal fractures in the plane strain mode, although their work preceded the detailed analysis of blunting given here.

Let us now examine some data. Pellissier and coworkers[18,19] report plane strain fracture toughness values for four alloy steels of essentially identical composition and yield stress level ($\sim$ 240 ksi), except for differences in sulfur content. Ample manganese was present to form rod-shaped manganese-sulfide particles, and it is reported that the steels were otherwise exceptionally free of nonmetallic inclusions. The fracture surface topography suggested ductile fracture by void growth from these inclusions. Table 1 lists in the first three columns the weight by percent of sulfur, measured stress intensity factor at fracture, and mean particle spacing (measured from a metallographic section) which we here identify as X_o. Using Eq. (8), the crack tip opening displacement as calculated from the K values appears in the next column, and the ratio δ_t/X_o in the last. These ratios are indeed in the anticipated

TABLE 1. δ_t at Fracture and Inclusion Spacing X_o for a High Strength Steel[18,19]

$wt.\%S$	$K(ksi\sqrt{in.})$	X_o (microns)	δ_t (microns)	δ_t/X_o
0.008	65	6.1	9.1	1.5
0.016	56	5.4	6.8	1.3
0.025	51	4.4	5.6	1.3
0.049	43	3.7	4.0	1.1

range, with the average ratio corresponding to a true strain at fracture of 0.3 at a distance equal to the particle spacing. Now let us turn to the aluminum alloy 7075-T6. Irwin[1] reports a value of $(1 - \nu^2)K^2/E$ at the fracture equal to 115 lb/in., with a 67 ksi yield stress, from which we compute $\delta_t = 26$ microns. Professor F. A. McClintock (private communication) reported a spacing of "larger" inclusions, with diameters 1–2 microns, in the range of 10–20 microns from his metallographic studies on this alloy. Taking the midvalue for X_o, we have $\delta_t/X_o = 1.7$ which is again in the expected range and corresponds to a true strain of about 0.5.

These two cases involve very high strength materials in their respective classes, both conforming about as closely as can be expected for real materials to the nonhardening idealization on which the theory is based. More generally, in view of the trend of increasing toughness with decreasing strength level and accompanying hardening[20] it would appear certain that values of δ_t/X_o would usually be closer to the upper end of the scale in Eq. (34). Both greater tenacity of inclusions to the matrix in lower stress fields and greater strains to void coalescence with hardening[16] may be factors. These, as well as hardening modifications of the strain distribution, cannot yet be treated. Indeed, McClintock reports that the smooth stretch zone preceding a ductile dimple fracture surface may extend a distance as great as 5 to 10 dimple diameters, and this would argue for higher values of δ_t/X_o if we interpret the stretch zone as a surface record of the blunting process.

We shall continue with the blunting solution given here as a basis for the discussion in following sections. However, we must caution that an important uniqueness question remains unresolved. As noted by Lee and Wang,[21] solutions of two types can be found for deformation at sharp-tipped notches in plane strain. One involves blunting of the tip into a smooth arc as derived here and shown in Figs. 5 and 6. It is also possible to find solutions in which the notch tip retains sharp corners with attached centered fans of singular

strain rates. In fact, the smooth tip solution may be viewed as the limit of solutions with a large number of corners. Even after the tip has begun to deform according to a solution of one type, it cannot be assured that this type of solution will persist. For example, a nick on a smoothly blunting tip may destabilize the solution, with subsequent growth exhibiting flow localization at a sharp corner. On the other hand, any solution with a sharp corner may be continued subsequently by a solution in which the corner blunts into a smooth arc. The distinction in a continuum description is that material points initially in the interior of the body may be brought to the surface in the sharp corner solutions, but not in the smooth tip solution. That is, localized deformation at sharp corners may be thought of as progressive "sliding off" of material to form fresh surfaces. Macroscopically flat plane strain fractures sometimes exhibit a zigzag appearance on a small size scale.[22] This might be a reflection of corner formation on a blunting crack tip, but might also be a consequence of the also large strains which occur at points off the symmetry line ahead of the tip.

4. MODEL FOR FRACTURE BY DUCTILE VOID GROWTH AT A CRACK TIP

We shall now dispense with the critical strain at a characteristic distance criterion, and attempt to directly calculate the crack opening displacement at fracture from a simple and highly approximate model for ductile fracture by void growth. Figure 8 shows an initially spherical cavity of radius R_o at a distance X_o from the tip of a sharp crack. We are going to employ the results of Rice and Tracey[23] for growth of an isolated cavity in a remotely uniform deformation field in a rigid-plastic material. The remote field of their analysis will be identified with the local stress and deformation field of the blunting analysis at the current void site, but computed as in the last section as if no void were present. Thus the calculations of growth, as the void site becomes enveloped by the large strain region (Fig. 8), are completely uncoupled. The strong interactions between neighboring free surfaces[12] are neglected, except for a very crude approximation adopted to describe final coalescence of the void with the crack, which we identify as "fracture."

For a sphere of radius R, the results for increments of radius measure in the x, y, and z directions, when adapted to the special case of a plane strain remote field duplicating that along the x axis ahead of the crack, are[21]

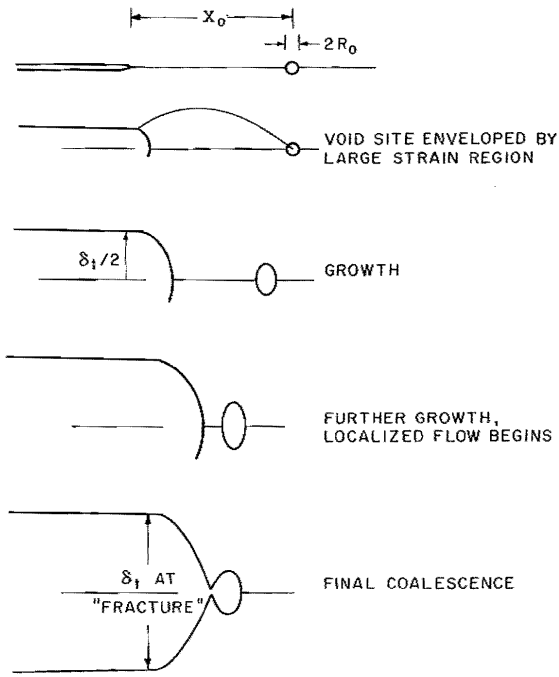

Fig. 8 *Model for ductile fracture by the growth and coalescence of an initially spherical void with the crack tip.*

$$\frac{dR_z}{R} = 0.322\, d\epsilon_y^{tr} \exp(\sqrt{3}\,\sigma/\tau_o)$$

$$\frac{dR_x}{R} = -2d\epsilon_y^{tr} + \frac{dR_z}{R} \qquad \frac{dR_y}{R} = 2d\epsilon_y^{tr} + \frac{dR_z}{R} \tag{35}$$

The equations are based on a Rayleigh-Ritz approximate solution from a variational formulation of the problem, and employ a further approximation appropriate for the moderate to high mean normal stress σ encountered in the present case. McClintock[16] noted a similar exponential amplification of void growth by the mean stress, and this is especially significant with the high triaxiality present in plane strain. We employ these equations even after the shape deviates from spherical, identifying R as the mean radius which is seen to equal R_z. In terms of the angle parameter ψ indicating position along the x axis ahead of the tip, $\sigma = (1 + 2\psi)\tau_o$ and ϵ_y^{tr} is given by Eq.

(33), so that

$$\frac{R_z}{R_o} = \exp\left\{0.322 \int_{\pi/2}^{\psi} \frac{\exp[\sqrt{3}(1 + 2\psi)/2]\, V'(\psi)}{F(\psi) - V(\psi)}\, d\psi\right\} \tag{36}$$

Similarly, R_x/R_o and R_y/R_o may be expressed in terms of ψ, and since $X_o = \delta_t H(\psi)$ from Eq. (31), the radius ratios may be expressed in terms of δ_t/X_o.

We adopt these equations up to the point where the distance between the void boundary and blunted crack tip is equal to the vertical radius R_y of the void, or from Eq. (29)

$$\delta_t [F(\psi) - F(0)] - R_x = R_y \tag{37}$$

with the first term representing distance from the crack tip to current void center location. Then it is assumed that final fracture occurs by a localized necking of the remaining ligament, requiring an additional opening displacement to fracture equal to the ligament size. It is necessary to invoke this localized flow, since the uncoupled equations would lead to an unrealistic stringing out of the void in the y direction with contraction in R_x prior to coalescence. The opening displacement at onset of flow localization is given in terms of X_o/R_o by rearranging Eq. (37) as

$$\frac{\delta_t}{X_o} [F(\psi) - F(0)] \frac{R_o}{R_x + R_y} = \frac{R_o}{X_o} \tag{38}$$

since the terms on the left are all known in terms of ψ and hence implicitly in terms of δ_t/X_o. The additional opening displacement assumed for the localized necking does not turn out to be a major contributor to the final opening displacement at fracture for X_o/R_o greater than 5 or so. Numerical results for δ_t/X_o at fracture are shown in Fig. 9 as a function of X_o/R_o, based on calculations for the small scale yielding and fully plastic input velocity fields.

The degree of accord of experimental results (Table 1) with this prediction will depend strongly on the choice of X_o and R_o from the given data. For example, if we continue to interpret X_o as the mean nearest neighbor spacing in a planar section and assume all particles are identical spheres, then $X_o/R_o = 0.72 f^{-1/2}$ where f is the volume fraction and statistical results quoted by Ashby and Ebeling[24] are

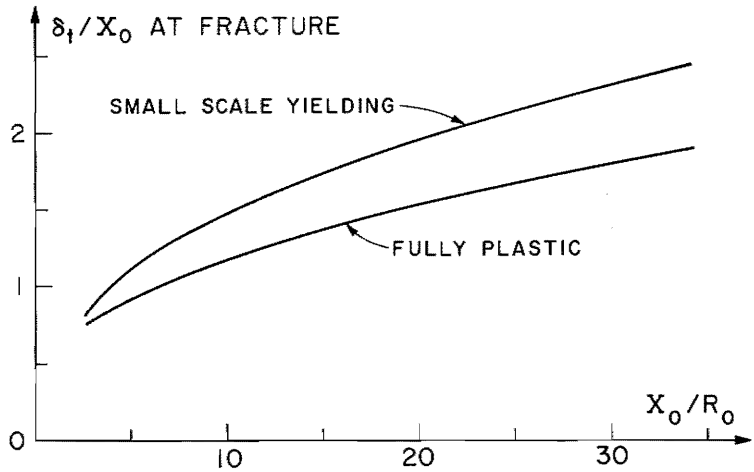

Fig. 9 *Predicted crack opening displacement at fracture, based on model in Fig. 8.*

used. The volume fraction can be computed from the percentage of sulfur by weight, assuming all sulfur present reacts with the more than ample manganese. From atomic weight ratios, wt %MnS = 2.7 (wt %S), and from specific gravity ratios of MnS and steel, vol %MnS = 2 (wt %MnS), so that $f = 0.054$ (wt %S). Thus, as we descend Table 1, X_o/R_o = 34, 24, 19, and 14. The general trend of δ_t/X_o ratios at fracture is therefore in accord with Fig. 9, but the relevant curve (marked "small scale yielding") is high by a factor of nearly two. On the other hand, if we choose R_o in the model to match the ratio of three-dimensional nearest neighbor distance to particle size with X_o/R_o, we have[24] $X_o/R_o = 0.89\, f^{-1/3} = 11.7$, 9.9, 8.0, and 6.5 as we descend Table 1, and a better agreement. Much further work is clearly needed, not only on the statistics, but also on interactions between neighboring free surfaces, on the effects of hardening, and on the tenacity of particles to the matrix (here assumed negligible for MnS particles is the triaxially elevated stress field ahead of the crack).

McClintock[22] has studied a similar ductile fracture model, combining his void growth predictions[16] with Wang's[12] results on notch tip deformation in the fully plastic case. He considers a row of uniformly spaced circular cylindrical cavities along the x axis ahead of the tip. His emphasis is on establishing the geometry of an advancing crack in a rigid plastic specimen under deformation boundary conditions, through relating the macroscopic angle of separation between advancing crack surfaces to the X_o/R_o ratio.

In comparison, our model is more precisely for the initiation of crack extension, with coalescence of the void in the model with the tip being taken to represent the many coalescence processes actually occurring along the crack front in the beginning stages of a fracture. Undoubtedly, the advancing crack is the more realistic fracture model, but only when analyzed with the elastic terms included so as to allow an instability. Crack advance in rigid-plastic models is necessarily stable.[17] We are unaware of observations of stable crack advance with plane strain small scale yielding conditions. Further, the data discussed earlier suggests that any crack advance under these conditions will be limited to that due to the blunting process itself, so that initiation of separation then appears to be the key event. Nevertheless, substantial stable crack advance is known to occur under nominally plane stress conditions and McClintock[22] reports cases of fully plastic plane strain specimens in which stable growth is also observed.

5. LARGE GEOMETRY CHANGE EFFECTS AND THE NEAR TIP STRESS STATE

We have seen that large geometry change effects are central to understanding ductile fracture through their modifications of the near tip strain distribution. Now we turn to their modifications of the stress state. Figure 4*b* suggests that hardening stress-strain relations lead to tensile stresses very near the tip which are substantially in excess of the already high $3\sigma_o$ value for perfect plasticity. However, it has been noted that at that point strains are small in the sgc solutions, and that the large stresses result from an enhanced ratio of hydrostatic to equivalent uniaxial components. Clearly, this enormous stress triaxility cannot be maintained at and near the blunted crack tip.

To examine the modified stress distribution, consider the x direction equilibrium equation

$$\frac{\partial \sigma_{xx}}{\partial x} + \frac{\partial \sigma_{xy}}{\partial y} = 0 \tag{39}$$

If we write this equation on the x axis directly ahead of the tip, noting that $\sigma_{xy} = 0$ there and following an approach similar to Bridgman's[25] tensile neck analysis, we have

$$\frac{\partial \sigma_{xx}}{\partial x} + (\sigma_{xx} - \sigma_{yy}) \left.\frac{\partial \phi}{\partial y}\right|_{y=0} = 0 \tag{40}$$

where ϕ is the angle of the first shear direction and hence $\partial\phi/\partial y$ is the curvature of principal stress trajectories as they cross the x axis. Not having a solution for large geometry changes in a hardening material, we shall make the following approximations: the deviatoric part of the stress state will be computed from the strain distribution in the nonhardening case, and the remaining part will be determined by integrating Eq. (40) subject to $\sigma_{xx} = 0$ on the blunted tip, with the curvature of principal stress trajectories in the nonhardening case substituted for $\partial\phi/\partial y$. The results will be exact in the nonhardening case, but certainly in substantial error for other than moderate strain hardening.

By Eq. (18), $\partial\phi/\partial y = \partial\alpha/\partial y + \partial\beta/\partial y$, and the latter two derivatives can be computed by standard means in terms of the set $\partial(x, y)/\partial(\alpha,\beta)$. Since shear angles cross at 45° on the x axis, we have $\partial y/\partial\alpha = \partial x/\partial\alpha$ and $\partial y/\partial\beta = -\partial x/\partial\beta$ there. Now, by symmetry considerations we may show $\partial x/\partial\alpha = -\partial x/\partial\beta$ on the axis and finally, using the representation of Eq. (29) for the x coordinate and expressing α and β in terms of the parameter angle ψ

$$\frac{\partial x}{\partial \psi} = \delta_t F'(\psi) = \frac{\partial x}{\partial \alpha}\frac{\partial \alpha}{\partial \psi} + \frac{\partial x}{\partial \beta}\frac{\partial \beta}{\partial \psi} = \frac{1}{2}\left(\frac{\partial x}{\partial \alpha} - \frac{\partial x}{\partial \beta}\right) \tag{41}$$

Omitting the algebraic details, the final result for the curvature is

$$\left.\frac{\partial \phi}{\partial y}\right|_{y=0} = \frac{1}{\delta_t F'(\psi)} \tag{42}$$

But $\partial/\partial x$ in the equilibrium equation may be written as $[\delta_t F'(\psi)]^{-1}\,\partial/\partial\psi$, and thus

$$\frac{\partial \sigma_{xx}}{\partial \psi} + \sigma_{xx} - \sigma_{yy} = 0 \qquad \text{with} \qquad \sigma_{xx} = 0 \text{ at } \psi = 0 \tag{43}$$

Let $\sigma = f(\epsilon^{tr})$ describe the true stress-strain relation in simple tension. Then adopting the Mises equivalent stress and strain forms, in the present plane strain case we have

$$\sigma_{yy} - \sigma_{xx} = \frac{2}{\sqrt{3}} f\left(\frac{2}{\sqrt{3}} \epsilon_y^{tr}\right) \tag{44}$$

The resulting prediction for tensile stress σ_{yy} acting on the x axis is therefore

$$\sigma_{yy} = \frac{2}{\sqrt{3}} f\left[\frac{2}{\sqrt{3}} \epsilon_y^{tr}(\psi)\right] + \frac{2}{\sqrt{3}} \int_0^{\psi} f\left[\frac{2}{\sqrt{3}} \epsilon_y^{tr}(\psi)\right] d\psi \tag{45}$$

where $\epsilon_y^{tr}(\psi)$ is given by Eq. (33).

Numerical results were obtained as based on the input velocity field from the sgc approximation for small scale yielding in Eqs. (8) and (9). These employ a power-law stress-strain relation

$$\sigma = f(\epsilon^{tr}) = \sigma_o \left(\frac{E\epsilon^{tr}}{\sigma_o}\right)^N \tag{46}$$

which we regard as a continuation of the linear elastic form as earlier. From Eq. (45), we can obtain $(\sigma_o/E)^N \sigma_{yy}/\sigma_o$ as a dimensionless function of ψ for each N. This can be converted through Eq. (31) to a function of X/δ_t, X being the coordinate of a material point before deformation. From Eq. (8), X/δ_t equals $1.63\ (E/\sigma_o)\, X/(K/\sigma_o)^2$. Thus, by selecting specific values of σ_o/E we can obtain the maximum stress to yield stress ratio σ_{yy}/σ_o as a function of the conventional distance parameter $X/(K/\sigma_o)^2$ in the region affected by blunting. These results are shown by the nonsolid lines in Fig. 10 for hardening exponents of $N = 0.0$, 0.1, 0.2 and for initial yield strains $\sigma_o/E = 0.0025$, 0.0050, 0.0075. The results are plotted out to a distance equal to the maximum extent of the blunting affected region. The solid lines shown are simply a replot of the Hutchinson-Rice-Rosengren hardening singularity solution in Fig. 4*b*. The match-up of the approximate modified stress distributions in the blunting affected region and the sgc distribution outside is surprisingly good.

There is actually a stress singularity predicted in the hardening cases at $X = 0$, but the singularity is so weak and dominates over such a small distance that the upturn in stress barely shows in the figure. The net conclusion is that with consideration of actual geometry changes at the crack tip, the maximum stress achievable over any reasonable size scale in the material is limited, contrary to

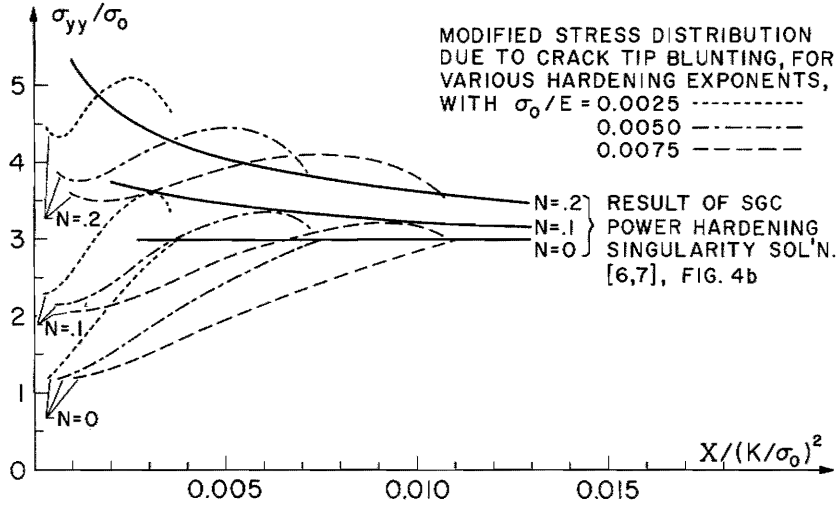

Fig. 10 *Nonsolid lines show approximate modified stress distribution due to large tip geometry changes, as dependent on initial yield strain σ_o/E and hardening exponent N. Conclusion is that maximum stress achievable over any reasonable size scale in the material is limited, contrary to sgc analysis.*

the conclusions which might be drawn from Fig. 4*b* of the sgc analysis. Maximum achievable stress levels can be estimated from Fig. 10 as a function of hardening exponent and initial yield strain, although the approximations probably give a progressive overestimate of stress in the blunting affected region with increasing hardening.

The concept of a maximum achievable stress is, of course, suggestive of abrupt toughness transitions with temperature or loading rate in materials capable of cleavage. For if we adopt the conventional model of a critical tensile stress for initiation of microcracking,[26] then clearly cleavage will be possible only if the maximum achievable stress associated with the yield and hardening characteristics of the material (as dependent on temperature and local strain rate) is sufficient to the task. Otherwise, ductile mechanisms must initiate the fracture, although these may serve as a precursor to cleavage due to enhanced local strain rates. Given that the maximum ~~achieved at least over a region comparable to one or a few grain diameters. Figure 10, when extended out to larger distances and corrected~~ achieved at least over a region comparable to one or a few grain diameters. Figure 10, when extended out to larger distances and corrected according to the much larger size scale plot of the stress fall-off in Fig. 4*b*, suggests that stress near the maximum achievable values can occur only over quite minute fractions of the length parameter $(K/\sigma_o)^2$.

achievable stress is sufficient ~~for~~ cleavage, size scale must also be considered in determining toughness, in that the critical stress must be

Locations of stress maxima in Fig. 10 suggest that a material point experiences the largest stresses before it becomes enveloped by the region of intense straining. Thus, for ductile fracture, it would appear that the particle failures creating void sites occur either in the precursor stress field or in the coalescence stages of other voids created in the precursor field. Probably the void spacing set by failures in the precursor field is the important size parameter for ductile fracture, although postmortem examination of fracture surfaces will not allow a distinction between the two.

6. CLOSURE

We have seen that consideration of the actual large geometry changes at a crack tip provides a view of fracture quite different from that afforded by the conventional sgc treatment. In particular, the intense strain region created ahead of the tip in blunting allows ductile fracture processes to operate there, and the analysis provides a reasonably coherent quantitative understanding. At the same time, the immense hydrostatic stress elevation is prohibited directly ahead, and maximum achievable stress levels are essentially limited. Many problems remain; some are basic and others call for refinement of the present analysis.

These problems include: clarification of smooth versus sharp-cornered notch tip deformation solutions, a more precise assessment of hardening effects, modeling of stable crack advance and instability, development of failure criteria for second phase particles, and inclusion of hardening and interaction effects in ductile void growth and coalescence models.

ACKNOWLEDGMENTS

Progress in this study has been greatly facilitated by many helpful discussions with Professor F. A. McClintock, particularly during his recent tenure as Visiting Professor at Brown University.

Financial support from the Atomic Energy Commission, under Contract AT(30-1)-2394, is gratefully acknowledged.

REFERENCES

1. Irwin, G. R.: in J. N. Goodier and N. J. Hoff (eds.), "Structural Mechanics," p. 557, Pergamon Press, 1960.
2. Paris, P. C., and G. C. Sih: "Fracture Toughness Testing and Its Applications," *STP*-381, p. 30, ASTM, Philadelphia, 1965.

3. Rice, J. R.: *J. Appl. Mech.*, 35:379 (1968).
4. Cherepanov, G. P.: *Prikl. Mat. Mekh.*, 31:476 (1967).
5. Rice, J. R.: in H. A. Liebowitz (ed.), "Treatise on Fracture," vol. 2, p. 191, Academic Press, 1968.
6. Hutchinson, J. W.: *J. Mech. Phys. Solids*, 16:13 (1968).
7. Rice, J. R., and G. F. Rosengren: *ibid.*, 16:1 (1968).
8. Ostergren, W. J. masters thesis, Brown University, March 1969.
9. Levy, N.: doctoral dissertation, Brown University, Jan., 1970.
10. McClintock, F. A., and G. R. Irwin: "Fracture Toughness Testing and Its Applications," *STP*-381, p. 84, ASTM, Philadelphia, 1965.
11. Hill, R.: "The Mathematical Theory of Plasticity," p. 151, Clarendon Press, Oxford, 1950.
12. Wang, A. J.: *Quart. Appl. Math.*, 11:427 (1953).
13. Rogers, H. C.: *Trans. Metall. Soc. AIME*, 218:498 (1960).
14. Gurland, J., and J. Plateau: *Trans. Am. Soc. Metals*, 56:442 (1963).
15. Beachem, C. D.: *Trans. Am. Soc. Metals*, 56:318 (1963).
16. McClintock, F. A.: *J. Appl. Mech.*, 35:363 (1968).
17. Drucker, D. C., and J. R. Rice: *Engr. Fracture Mech.*, to be published.
18. Birkle, A. J., R. P. Wei, and G. E. Pellissier: *Trans. Am. Soc. Metals*, 59:981 (1966).
19. Pellissier, G. E.: *Engr. Fracture Mech.*, 1:55 (1968).
20. Krafft, J. M.: *Appl. Materials Res.*, 1964:88.
21. Lee, E. H., and A. J. Wang: *Proc. 2d U.S. Nat. Cong. Appl. Mech.*, p. 489, ASME, New York, 1954.
22. McClintock, F. A.: in A. S. Argon (ed.), "Physics of Strength and Plasticity," p. 307, M.I.T. Press, 1969.
23. Rice, J. R., and D. M. Tracey: *J. Mech. Phys. Solids*, 17:201 (1969).
24. Ashby, M. F., and R. Ebeling: *Trans. Metall. Soc. AIME*, 236:1396 (1966).
25. Bridgman, P. W.: "Large Plastic Flow and Fracture," p. 9, McGraw-Hill Book Company, New York, 1952.
26. Wilshaw, T. R., C. A. Rau, and A. S. Tetelman: *Engr. Fracture Mech.*, 1:191 (1968).

DISCUSSION *on Paper Presented by J. R. Rice*

J. E. SRAWLEY: In relation to the values of δ_t for plane strain fracture cited by Professor Rice, and the ratios of these to the mean inclusion spacing, I want to call his attention to some values for maraging steel from my laboratory. By varying the maraging temperature and/or time, the yield strength can be raised over a range, for example, from 150 to 260 ksi for a so-called 250-grade composition. The K_{Ic} toughness varies inversely with the yield strength, and the values of $\delta_t (= 0.6 K_{Ic}^2/E\sigma_{YS})$ range from 15 microns to at least 75 microns. Because the inclusion distribution is not affected by the maraging treatment, δ_t is independent of the mean inclusion spacing. Moreover, the hardening precipitate particles are extremely small and closely spaced (much less than one micron). So far no one has been able to establish the identity of the void-nucleating particles in these materials.

J. R. RICE: It is, of course, necessary that the microstructural dimension to which δ_t is compared be relevant to the fracture mechanism. As Dr. Srawley notes in his last sentence, it is not

clear that the spacing of hardening precipitate particles in maraging steels is a relevant dimension. Similarly, the steel on which Table 1 is based contained cementite particles as well as the larger MnS particles, but evidently only the latter were important in nucleating the fractures.[1,2] This emphasizes the importance of better understanding particle separations and other possible void nucleation mechanisms.

We have commented in the text on the sort of variation of δ_t at fracture with yield stress and hardening, for an essentially fixed microstructure, reported by Dr. Srawley. Both stress dependence of the density of void nucleation sites and inhibition of growth by hardening are in accord with observed trends, although no detailed theory is available. It is also possible that the instability point, in a process of quasi-static crack advance by void coalescence, will depend sensitively on the yield stress, as suggested by the antiplane shear analysis of elastic-plastic crack instability.[3]

A. R. ROSENFIELD: Metallographic studies of the ductile fracture process provide two useful observations which should be included in further development of the large crack tip radius model presented in this paper:

1. In unnotched tensile bars the true strain to fracture depends principally on the volume fraction of second phase particles and not only on their spacing as assumed by the authors. However, if the particle size is "too small" (e.g., $\lesssim 0.1\ \mu$) reductions-in-area on the order of 100 per cent are observed.

2. Particles most often begin to crack and/or separate from the matrix at very low plastic strains.

The model suggested by these observations is one in which holes exist throughout the plastic zone. The size of these holes is the particle diameter and their spacing is the particle spacing. In essence the large strain region is a "Swiss cheese" whose characteristic dimensions are those of the microstructure.

J. R. RICE: The first point is not at all at variance with our ductile void growth model. The difference is that in the tensile test one is concerned with macroscopic strain fields that vary little over a mean particle spacing, whereas there is a very steep gradient over the same distance when the particle is directly ahead of the crack tip. In fact, since continuum plasticity contains no characteristic length, it is clear that an analysis paralleling ours for void growth and coalescence in a macroscopically homogeneous deformation field will lead to a fracture strain dependent on particle spacing and size solely through dimensionless ratios such as volume fraction. This distinction between stress and deformation fields

that are uniform and those that are nonuniform over typical microstructural dimensions seems basic for clarification of size effects in fracture.

In response to the second point, it certainly must be agreed that *some* particles fail early in the plastic stage. It seems important, however, to clarify just what fraction fails as a function of the stress and strain history achieved at points ahead of the crack, as this may be related to understanding toughness variations with yield and hardening behavior.

REFERENCES

1. Birkle, A. J., R. P. Wei, and G. E. Pellissier: *Trans. Am. Soc. Metals,* 59:981 (1966).
2. Pellissier, G. E.: *Engr. Fracture Mech.,* 1:55 (1968).
3. Rice, J. R.: in H. A. Liebowitz (ed.), "Treatise on Fracture," vol. 2, p. 191, Academic Press, 1968.